A Proposal to JLab PAC 42, a companion to the WACS Proposal

Wide Angle, Exclusive Photoproduction of π^0 Mesons

J. Dunne, D. Dutta (Co-spokesperson and contact person), L. El Fassi, J. Madsen, A Narayan, L. Ndukum, A. Subedi, L. Ye

Mississippi State University, Mississippi State, MS

P. Chu, H. Gao (Co-spokesperson), M. Huang, G. Laskaris, X. Li, M. Meziane, C. Peng, W. Xiong, X. Yan, Z. Ye, Y. Zhang

Duke University and Triangle University Nuclear Lab, Durham, NC

J. Beričič, S. Širca (Co-spokesperson), S. Štajner

Jožef Stefan Institute and University of Ljubljana, Ljubljana, Slovenia

M. Amaryan (Co-spokesperson), C. E. Hyde, M. Kunkel (Co-spokesperson)

Old Dominion University, Norfolk, VA

W. J. Briscoe, M. U. Doering, I. Strakovsky (Co-spokesperson) and R. L. Workman

George Washington University, Washington, DC

A. Camsonne, S. Covrig, R. Ent, D. Gaskell, G. Gavalian, M. K. Jones, C. Keppel, D. Mack, B. Wojtsekhowski, S. A. Wood

Jefferson Lab, Newport News, VA

I. Albayrak, M. A. Pannunzio Carmignotto, J. Denes-Couto, N. Hlavin, T. Horn, F. Klein, B. Nepal

The Catholic University of America, Washington, DC

R. Lindgren

University of Virginia, Charlottesville, VA

S. Abrahamyan, A. Asaturyan, A. Mkrtchyan, H. Mkrtchyan, V. Tadevosyan, A. Shahinyan, H. Voskanyan, S. Zhamkochyan
A.I. Alikhanyan National Science Laboratory, Yerevan, Armenia

P.M. King, J. Roche
Ohio University, Athens, OH

Nuruzzaman
Hampton University, Hampton, VA

A. Ahmidouch, S. Danagoulian
North Carolina A&T University, Greensboro, NC

M. Elassar
Southern University at New Orleans, New Orleans, LA

K. Aniol
California State University, Los Angeles, CA

M. Paolone
Temple University, Philadelphia, PA

Z. Ahmed, G.M. Huber, W. Li, D. Paudyal
University of Regina, Regina, SK, Canada

The Wide Angle Compton Scattering (WACS) collaboration
and
the Neutral Particle Spectrometer (NPS) collaboration

Hard exclusive reactions provide an excellent opportunity to study the complicated hadronic dynamics of underlying subprocesses at partonic level. The Wide Angle Compton Scattering (WACS) and exclusive photoproduction of mesons with large values of energy and momentum transfers ($s \sim t \sim u \gg \Lambda$) are among the most elementary reactions due to minimal total number of constituent partons involved in these $2 \to 2$ reactions. Existing world data on photoproduction of neutral pions on proton $\gamma + p \to \pi^0 + p$ have very large systematic errors and do not have sufficient accuracy to perform comprehensive phenomenological analysis. Preliminary expermimental data from CLAS on π^0 photoproduction extend existing world precise measurements of differential cross section up to $s \sim$11 GeV^2.

We propose to measure the differential cross section of the $\gamma p \to \pi^0 p$ process in the range of 10 GeV^2 $< s <$20 GeV^2 at large pion center-of-mass angles of $55^\circ < \theta_{cm} < 105^\circ$. The proposed measurements will be carried out in Hall C using an electron beam impinging on a 6% copper radiator and a liquid hydrogen target. The recoil proton will be detected in the HMS spectrometer and photons from the $\pi^0 \to \gamma\gamma$ decay will be detected in the Neutral Particle Spectrometer (NPS) which is under construction. The scattered electrons will be deflected by using a sweeping magnet.

This is a companion to the proposed wide angle Compton scattering (WACS) experiment. π^0 photo production differential cross section will be extracted from the same data set that is collected by the WACS experiment. In addition to all of the settings of the WACS experiment measurements at a beam energy of 6.6 GeV will be required for the proposed experiment to overlap with existing data.

CONTENTS

1. INTRODUCTION

Exclusive processes at large momentum transfers and wide angles ($p_T \geq 1GeV/c$) are essential for studies of the short range structure of nucleons. They provide a robust testing ground for QCD at intermediate energies which is one of the main goals of the physics program at JLab. Towards this goal, wide angle exclusive processes can be used to test recent developments, such as the framework based on the dominance of the "handbag mechanism" and models based on Generalized Parton Distribution (GPD) [1]. Given the relatively large cross sections for pion photoproduction, a confirmation of the dominance of the handbag mechanism would enable a study of the nucleon structure at large values of W and $-t$.

The handbag mechanism for wide-angle scattering reactions was first developed for Compton scattering [2, 3] and subsequently applied to photo- and electroproduction of mesons [4]. Several new calculations on wide-angle Compton scattering have recently become available [5–8] and they can reproduce the measured cross sections. After Compton scattering, pion photoproduction is the next simplest real photon induced exclusive process. Although calculations of the pion photoproduction cross sections tend to disagree with experiments by orders of magnitude, the charged pion ratios seem to agree with calculations at the highest energies [9]. The current situation can only be remedied with a new measurements that employs a new technique with a new high resolution and radiation hard neutral pion detector [10] along with the high luminosity that will be available at JLab Hall-C. Since the neutral pion is one of the dominant physics backgrounds for the proposed WACS experiment, this proposal uses the exact same setup and is a companion to the WACS proposal [11]. The experimental sections describing the apparatus and analysis methods and several figures used in those sections have been reproduced from the WACS proposal with the permission of the WACS spokespeople.

Wide-angle exclusive processes can also help understand the transitions from the non-perturbative to perturbative regime of QCD. The differential cross sections for many exclusive reactions [12] at high energy and large momentum transfer appear to obey the quark counting rule [13]. The quark counting rule was originally obtained based on dimensional analysis of typical renormalizable theories. The same rule was later obtained in a short-distance perturbative QCD approach by Brodsky and Lepage[14]. Despite many successes, a model-independent test of the approach, called the hadron helicity conservation rule, tends not to agree with data in the similar energy and momentum region. It has been suggested that contributions from nonzero parton orbital angular momentum could break the hadron helicity conservation rule [15], although these contributions are power suppressed [14]. In addition some of the cross-section data can also be explained in terms of non-perturbative calculations [16]. Other developments over the last decade, such as the generalized counting rule proposed by Ji *et al.* [17], the derivation of the quark-counting rule from the anti-de Sitter/Conformal Field Theory (AdS/CFT) correspondence [18], and the machinery to compute the hadronic light front wave functions developed by Brodsky *et al.* [19], have focused interest back on this subject.

Current status of experimental data on photo production of π^0 is summarized in Fig. 1 for center of mass angles $\theta = 50^\circ, 70^\circ, 90^\circ, 110^\circ$. Low energy data are from MAMI [20] (in magenta) and CLAS g1c [21] (blue points). Higher energy range measurements are preliminary CLAS data from g12 experiment [22] (red points). Data from old measurements with bremsstrahlung beams [23] (open circles) with very large systematic errors are also presented for completeness.

By fitting g12 data at $\theta = 90^\circ$ by power law function s^{-n} we obtained $n = 6.89 \pm 0.26$. The same power law function is also superimposed on data taken at $50^\circ, 70^\circ$ and 110° degrees. As one can see experimental data at lower angles tend to reach power law behavior at much higher energies. One reason for this behavior

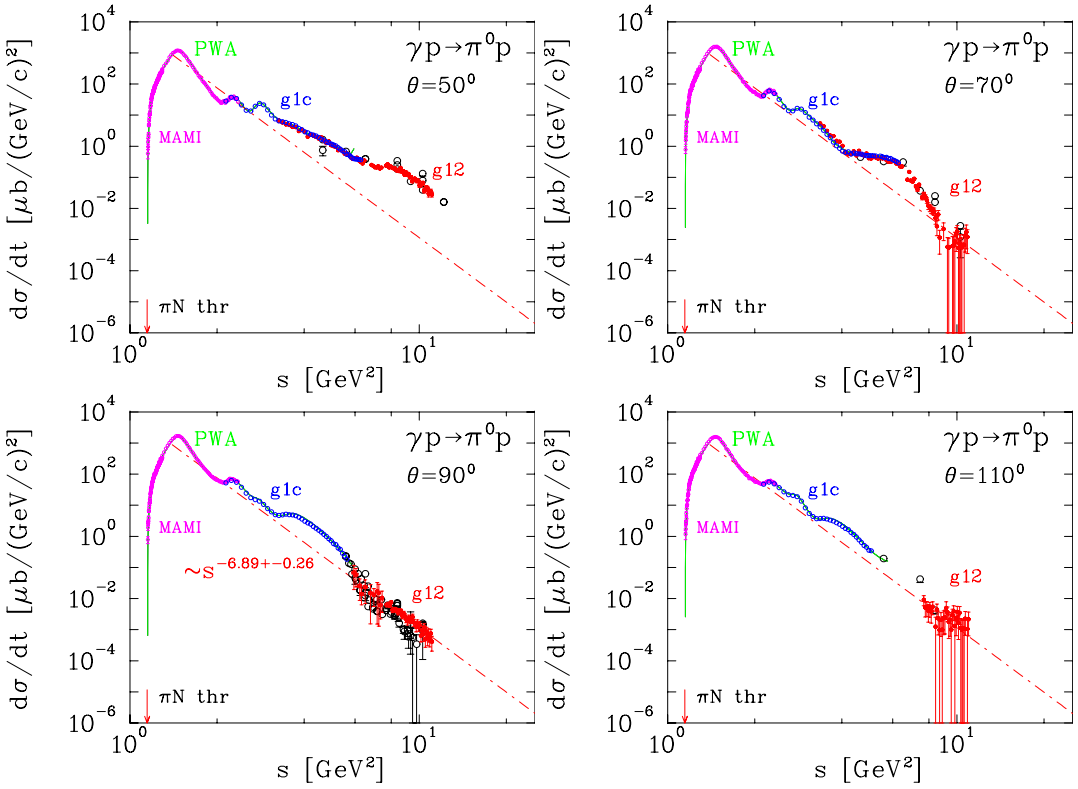

FIG. 1. The differential cross section for the $\gamma p \to \pi^0 p$ reaction at $\theta_{cm} = 50°, 70°, 90°, 110°$, as a function of the center of mass energy squared. The data are from Ref. [20], [21] and [22], open circles are data from old measurements [23]. The red points are preliminary results from a recent analysis of the CLAS g12 data. At high energies and large angles the results are consistent with the s^{-7} scaling expected from the quark counting rule. The dash dotted line is a result of the fit performed at $\theta = 90°$ with power function $\sim s^{-n}$ leading to $n = 6.89 \pm 0.26$.

may be due to different t ranges depending on the center of mass angle at fixed s as presented in Fig. 2. At lower angles t values are much smaller than s in the range of this data, therefore condition of counting rule [13], which requires large values of all three Mandelstam variables $s \sim t \sim u \gg \Lambda(QCD)$, is not fulfilled. The charged

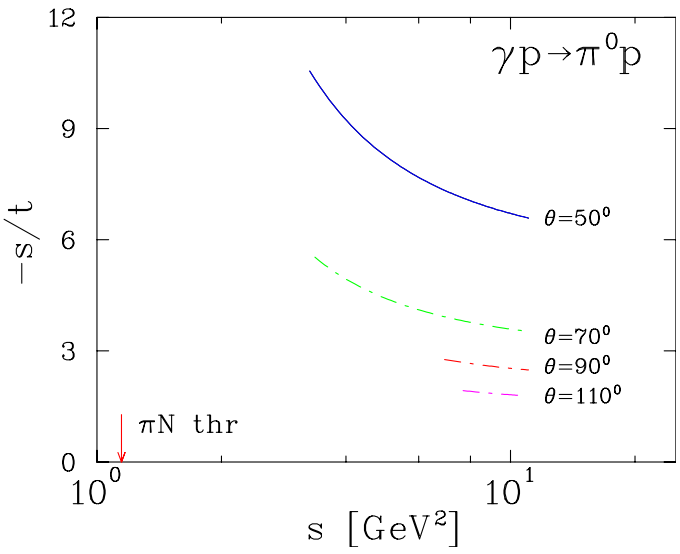

FIG. 2. s/t ratio for different center of mass angles as a function of invariant energy s.

pion photoproduction data at the highest energies also indicate a similar s^{-7} power law trend as is seen in Fig. 3.

The scaling behavior has been studied extensively in deuteron photo-disintegration experiments at SLAC and JLab [30] - [33]. Onset of the scaling behavior has been observed [32, 33] at a surprisingly low momentum transfer of 1.0 $(\mathrm{GeV/c})^2$ to the nucleon. Scaling behavior has also been observed in pion photoproduction, most recently in neutral pion production as shown in Fig. 1. However, polarization measurements on deuteron photo-disintegration [34] and in neutral pion photoproduction [35, 36], show disagreement with hadron helicity conservation in the same kinematic region where the quark counting behavior is apparently observed. These paradoxes make it essential to understand the exact mechanism governing the early onset of scaling behavior. Towards this goal, it is important to look closely at claims of agreement between the differential cross section data and the quark counting prediction and also to examine it over large angular range.

A large fraction of the pion photoproduction data at the highest energies have

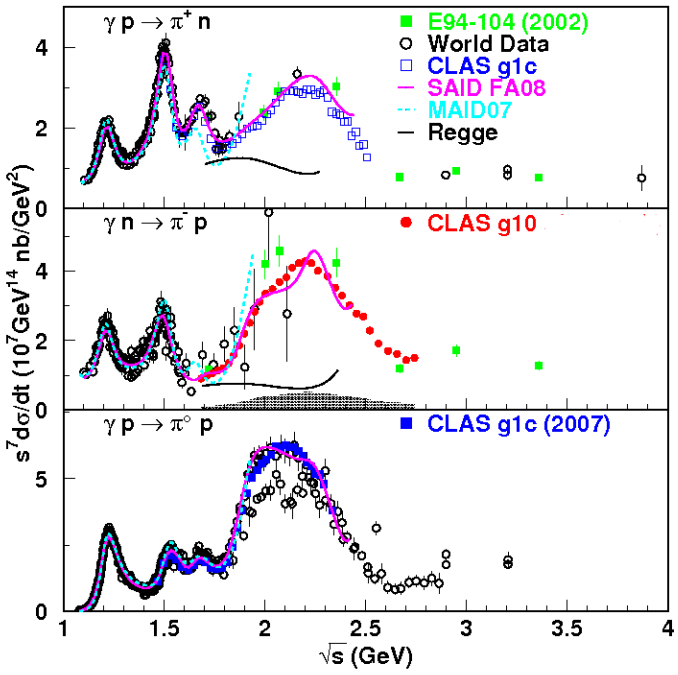

FIG. 3. The scaled differential cross section, $s^7 \frac{d\sigma}{dt}$ as a function of $\sqrt{s}$ at a center-of-mass angle of 90° for $\gamma p \to \pi^+ n$ channel (top panel), the $\gamma n \to \pi^- p$ channel (middle panel) and $\gamma p \to \pi^0 p$ (bottom panel). The data from JLab E94-104 are shown as green solid squares [24] and the CLAS π^+ data [21] are shown as magenta open squares, the π^- results [25] are shown as red solid circles and the π^0 results [21] are show as magenta solid squares. The SAID SP09 results [26] are shown as the blue solid curves in all three panels. The prediction from a Regge approach [27] is shown in the top and middle panels by black solid curves. The black open circles are the world data collected from Refs. [28, 29]

been collected using the "bremsstrahlung end point" technique. At the upgraded JLab, because of the fixed electron beam energy the end point technique would be restricted to very narrow range of energies and is thus no longer very effective. A high resolution, radiation-hard neutral particle detection facility will provide an

alternative method to measure wide angle π^0 photoproduction. The Neutral Particle Spectrometer under construction in Hall-C exactly fits the bill and will enable us to test the reaction mechanism of π^0 photoproduction. We propose to measure the differential cross-section $\frac{d\sigma}{dt}$ for the $p(\gamma, \pi^0)p$ processes over a range of center-of-mass angles in a photon energy between 5.0 and 10 GeV. We propose to use the data collected by the WACS experiment [11] at $E_{beam} = 8.8$ and 11.0 GeV to extract the π^0 cross section which is the largest source of physics background for the WACS experiment. In addition we propose to use the setup of the WACS experiment for additional measurements with 6.6 GeV electron beam at $70^\circ \leq \theta_{cm} \leq 105^\circ$ and one additional kinematics at 90° c.m. angles at $E_{beam} = 11$ GeV. Using the high luminosity and energy upgraded CEBAF, one can test the dominance of the handbag mechanism in pion photoproduction and also investigate its scaling behavior in detail to help identify the exact nature and the underlying mechanism responsible for scaling.

2. PHYSICS MOTIVATION

The main physics goals for measuring the π^0 cross section using the new NPS facility are to address the following questions:

1. Does the exclusive photopion production reaction proceed through the interaction of the photon with a single quark?

2. What is the energy scale for the transition from non-perturbative to pertubative mechanisms and/or soft to hard factorization mechanisms?

3. What can we learn about the non-perturbative structure of the proton using wide angle exclusive processes in general and pion photoproduction in particular?

We briefly discuss the current status of pion photoproduction models and the existing data and what is needed to be able to address the questions posed above.

2.1. The Handbag Mechanism and GPD-based Models

The introduction of the handbag mechanism has provided new possibilities for the interpretation of hard exclusive reactions. In this approach, the reaction is factorized into two parts, one quark from the incoming and one from the outgoing nucleon participate in the hard sub process, which is calculable using pQCD. While the soft part consists of all the other partons that are spectators and can be described in terms of GPDs [1]. This is illustrated in Fig. 4, where the hard exclusive meson (M) photo-production process factorizes into, $\gamma + q \rightarrow Mq$ and GPDs describing the soft hadronparton transitions. The handbag mechanism is applicable when the Mandelstam variables, s, t, u, are large as compared to a hadronic scale of order $1\ GeV$. The GPDs contain a wealth of information about the transverse distance and angular momentum of the quarks in the proton. They provide a unified description of nucleon structure, a common framework that can be applied to inclusive, semi-inclusive, and exclusive reactions. Presently, experimental access to such GPDs

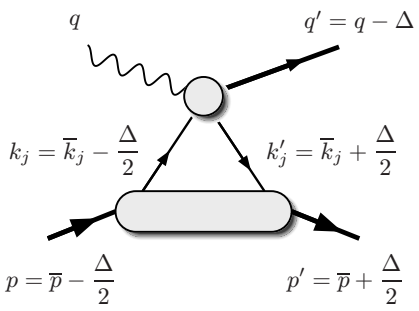

FIG. 4. The handbag diagram for photoproduction of mesons. The large blob represents a baryon GPD, while the small one stands for meson photoproduction off quarks.

is amongst the highest priorities in intermediate energy nuclear/particle physics. However, access to the GPDs is intrinsically related to the soft-hard factorization. All order proofs of factorisation exists only for deeply virtual processes. Factorization is particularly simple in the wide-angle processes, where it has been shown to hold to next-to-leading order in Compton scattering and to leading order in photoproduction of mesons. However, it is still uncertain at which Q^2 value one will reach the factorization regime, where leading-order perturbative QCD is fully applicable.

Recently, a new GPD based calculation by Diehl and Kroll [8] for wide angle Compton scattering, has been shown to agree well with experimental data.

The photoproduction of neutral pions at large c.m. angles is the next simplest reaction that can be tested against these GPD models. In ref. [4] the GPD based model of ref. [8] has been applied to predict angular dependence of scaled photoproduction cross section of π^0, presented in Fig. 5 (left panel). Preliminary experimental data from g12 CLAS run period [22] are presented on the right panel. The theoretical predictions are several orders of magnitude lower than experimental data.

One of the reasons for this failure may be due to one-gluon exchange mechanism for the generation of the meson and not the handbag mechanism itself. Although, the cross sections do not match experiments, H.W.Huang *et al.*, have also calcu-

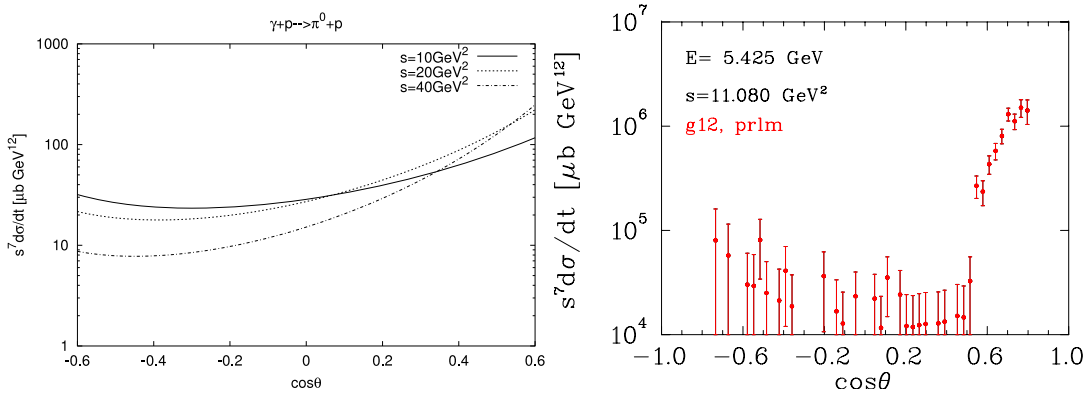

FIG. 5. Left panel is Fig.7 from [4]. Right panel- preliminary experimental data from CLAS [22]

.

lated other signatures of the handbag mechanism in wide-angle photoproduction of pseudoscalar mesons [9].

In their calculating of the $\pi^{\pm}$ cross sections ratio, the form factors cancel out and neglecting quark helicity flip contributions they obtain [9];

$$\frac{d\sigma(\gamma n \to \pi^- p)}{d\sigma(\gamma p \to \pi^+ n)} = \left(\frac{e_u s + e_d u}{e_u u + e_d s}\right)^2 . \tag{1}$$

This result coincides with the leading-twist prediction and are in surprisingly good agreement with experimental results from JLab [24] (see Fig. 6). It is surprising given the small photon beam energies involved.

Thus, there is an indirect indication from experiment that the handbag mechanism may be at work in these processes under the assumption of negligible quark helicity flip contributions.

The same formalism can be used to obtain the $\pi^0/\pi^{\pm}$ cross section ratios, however, in this case the form factors do not cancel out and a model of the form factors must be used to obtain the ratio. The predicted ratio for $\pi^0/\pi^{\pm}$ also disagree with data by about an order of magnitude, just as the measured cross sections disagree with

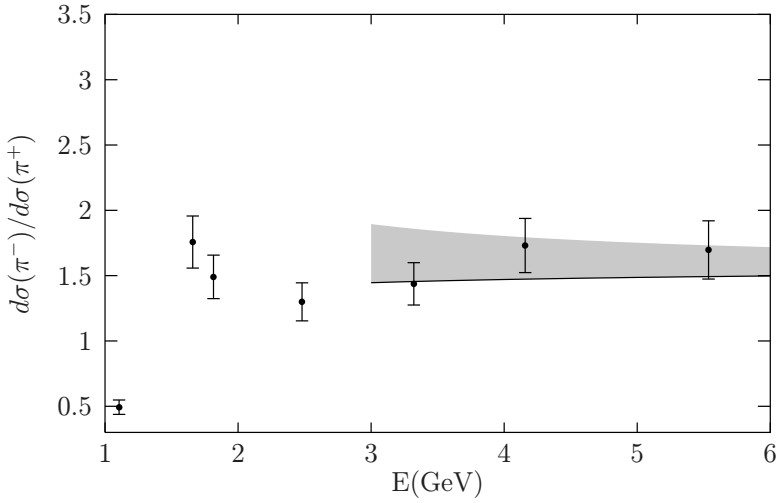

FIG. 6. The ratio of the $\gamma n \to \pi^- p$ and $\gamma p \to \pi^+ n$ cross sections versus photon beam energy E, at a c.m.s. scattering angle of 90°. Data are taken from [24]. The solid line is the handbag prediction, with the uncertainties due to target mass corrections is indicated by the shaded band.

the calculations.

Several new calculations on wide-angle Compton scattering have recently become available [5], [6], [7], [8] and they can reproduce the measured cross sections. In case of π^0 photoproduction not only theory must be further developed, but also a new higher precision measurements of the π^0 cross sections in wide energy and angular range are needed to resolve the discrepancy and to motivate calculations of the π^0 cross section that would help verify the dominance of the handbag mechanism and/or help identify missing dynamical mechanisms of π^0 photoproduction.

2.2. Constituent Counting Rule

The constituent counting rule predicts the energy dependence of the differential cross section at fixed center-of-mass angles for an exclusive two-body reaction at

high energy and large momentum transfer as follows:

$$d\sigma/dt = h(\theta_{cm})/s^{n-2}, \tag{2}$$

where s and t are the Mandelstam variables, s is the square of the total energy in the center-of-mass frame and t is the momentum transfer squared in the s channel. The quantity n is the total number of elementary fields in the initial and final states, while $h(\theta_{cm})$ depends on details of the dynamics of the process. In the case of pion photoproduction from a nucleon target, the quark counting rule predicts a s^{-7} scaling behavior for $\frac{d\sigma}{dt}$ at a fixed center-of-mass angle.

The quark counting rule was originally obtained based on dimensional analysis under the assumptions that the only scales in the system are momenta and that composite hadrons can be replaced by point-like constituents. Implicit in these assumptions is the approximation that the class of diagrams, which represent on-shell independent scattering of pairs of constituent quarks (Landshoff diagrams) [37], can be neglected. Also neglected were contributions from quark orbital angular momentum, which are power suppressed but can give rise to hadron helicity flipping amplitudes. These counting rules were also confirmed within the framework of perturbative QCD analysis up to a logarithmic factor of α_s and are believed to be valid at high energy, in the perturbative QCD region. Such analysis relies on the factorization of the exclusive process into a hard scattering amplitude and a soft quark amplitude inside the hadron. It has also been demonstrated that the counting rules for hard exclusive processes can arise from the correspondence between the anti-de Sitter space and conformal field theory [18] which connects superstring theory to superconformal gauge theory.

Many exclusive reactions [12, 28] at high energy and large momentum transfer appear to obey the CCR. A similar trend, i.e. global scaling behavior, has been observed in deuteron photo-disintegration experiments [31–33] and in photo-

production of charged pions [24] at a surprisingly low transverse momentum value of ~ 1.1 $(\mathrm{GeV/c})^2$. The other natural consequence of pQCD: the helicity conservation selection rule, tends not to agree with data in the experimentally tested region. Hadron helicity conservation arises from quark helicity conservation at high energies and the vector gluon-quark coupling nature of QCD and by neglecting the higher orbital angular momentum states of quarks or gluons in hadrons. The same dimensional analysis which predicts the quark counting rule also predicts hadron helicity conservation for exclusive processes at high energy and large momentum transfers. If hadron helicity conservation holds, the induced polarization of the recoil proton in the unpolarized deuteron photo-disintegration process is expected to be zero. Polarization measurements in deuteron photo-disintegration[34] and π^0 photoproduction [35, 36] have been carried out at JLab. For deuteron photo-disintegration, while the induced polarization does seem to approach zero around a photon energy of 1.0 GeV at 90° center-of-mass angle, the polarization transfer data are inconsistent with hadron helicity conservation. The results from π^0 photoproduction are also inconsistent with hadron helicity conservation.

The entire subject is very controversial. Isgur and Llewellyn-Smith [16] argue that if the nucleon wave-function has significant strength at low transverse quark momenta ($k_\perp$), then the hard gluon exchange (essential to the perturbative approach) which redistributes the transferred momentum among the quarks, is no longer required. The applicability of perturbative techniques at these low momentum transfers is in serious question. There are no definitive answers to the question-*what is the energy threshold at which pQCD can be applied?* Indeed the exact mechanism governing the observed quark counting rule behavior remains a mystery.

2.3. New Developments

A number of developments have generated renewed interest in this topic. For example, Zhao and Close [38] have argued that a breakdown in the locality of quark-hadron duality (dubbed as "restricted locality" of quark-hadron duality) results in oscillations around the scaling curves predicted by the counting rule. They explain that the smooth behavior of the scaling laws arise due to destructive interference between various intermediate resonance states in exclusive processes at high energies, however at lower energies this cancellation due to destructive interference breaks down locally and gives rise to oscillations about the smooth behavior.

On the other hand, Ji *et al.* [17] have derived a generalized counting rule based on pQCD analysis, by systematically enumerating the Fock components of a hadronic light-cone wave function. Their generalized counting rule for hard exclusive processes include parton orbital angular momentum and hadron helicity flip, thus they provide the scaling behavior of the helicity flipping amplitudes. The interference between the different helicity flip and non-flip amplitudes offers a new mechanism to explain the oscillations in the scaling cross-sections and spin correlations. Brodsky *et al.* [19] have used the anti-de Sitter/Conformal Field Theory correspondence or string/gauge duality [18] to compute the hadronic light front wave functions exactly and it yields an equivalent generalized counting rule without the use of perturbative theory. In a further test of these approaches, calculations of the nucleon form factors including quark orbital angular momentum in pQCD [39] and those computed from light-front hadron dynamics [19] both seem to explain the $\frac{1}{Q^2}$ fall-off of the proton form factor ratio, $G_E(Q^2)/G_M(Q^2)$, measured at JLab in polarization transfer experiments [40].

As mentioned earlier, the π^0 photoproduction is one of the few exclusive processes where the scaling behavior had not been verified and there is a lack of consistent data at high values of Mandelstam variables (s, t and u). Preliminary results from

CLAS [22] seem to suggest the onset of scaling at 90° c.m. angle. Thus, to verify the scaling of the cross-section of neutron pion photoproduction process and to understand its origin, it is imperative that we do a scan of the scaling region for the $\gamma p \to \pi^0 p$ processes and extend measurements to much higher center-of-mass energies over a range of center-of-mass angles. Using the high resolution (position and energy) calorimeter under construction in Hall-C one can scan over larger energy and angular range and help verify the scaling behavior and study its origins.

2.4. Summary of motivations

The π^0 cross sections at wide angles and large momentum transfers will provide tests of the dominance of handbag mechanism. They will also help identify any missing dynamical mechanism in the handbag approach.

The π^0 cross sections will help study the details of the energy and angular dependence of the scaling and help understand the exact mechanism behind the relatively early onset of scaling. It will also help investigate the details of the agreement with scaling laws and provide insight into any oscillations about the scaling behavior.

All of these results will help identify the the energy scale for the transition from the soft to hard factorization regimes and help understand the non-pertubative structure of the proton.

3. THE PROPOSED MEASUREMENT

We propose to carry out a measurement of the photo-pion production cross-section for the fundamental process $\gamma p \to \pi^0 p$ on a liquid hydrogen target over a pion center-of-mass angle ranging between $55^o < \theta_{cm} < 105^o$, and $\sqrt{s}$ over a range of $E_\gamma \sim 6$ GeV to 10 GeV. The π^0 photoproduction is the dominant background for the WACS experiment. Thus we propose to use the same setup as the WACS

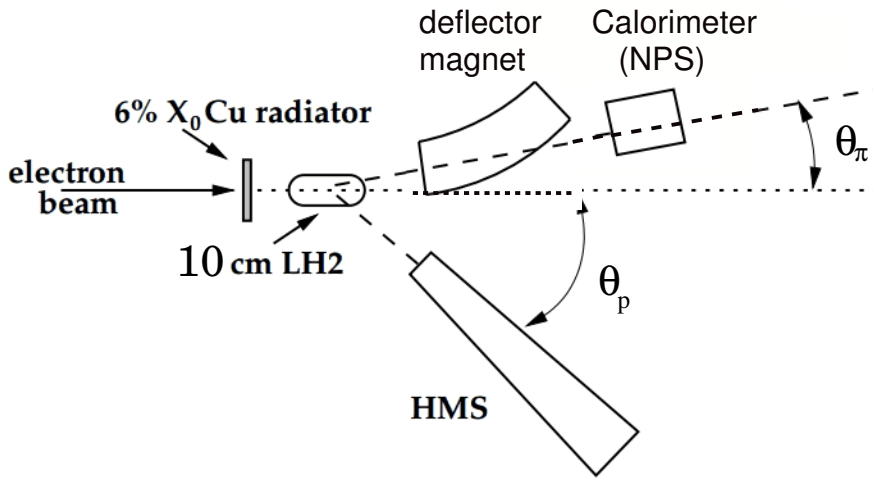

FIG. 7. Schematic of the experimental setup. This figure is reproduced from the WACS proposal with permission.

.

experiment and extract the π^0 cross section from the same data which is collected during the WACS experiment. The recoil protons will be detected in the High-Momentum Spectrometer (HMS) in standard configuration. The photons from he π^0 decay will be detected by the Neutral Particle Spectrometer (see Fig. 7). All of the key equipment is briefly mentioned here with detailed descriptions available in the WACS proposal [11].

3.1. The CEBAF Electron Beam

The maximum electron beam energy required is 11 GeV, in addition beam energies of 8.8 GeV and 6.6 GeV are also required. Beam with currents up to 60 μA will be used on a 10 cm long liquid hydrogen target. This implies an average luminosity of $\mathcal{L}_{ep} = 1.6 \ \times 10^{38}/cm^2/s$.

3.2. Target and Radiator

The experiment will utilize one of the standard Hall C liquid hydrogen (LH2) targets with a 10 cm-long machined cell with aluminum walls of 5 mm thickness, which has been successfully employed in many experiments at JLab. The copper radiator with a thickness of $t_{rad}/X_0 = 0.06$ (6% of radiation length) will be mounted on the cell block about 25 cm upstream of the cell entrance window. The distance between the target and the radiator and the high photon energies help avoid the background produced on the walls of the target and keeps the photon beam spot compact, which allows both accurate measurement of the proton momentum with the vertical bend spectrometer and operation with high luminosity. Further, the distance between the radiator and the target allows additional shielding to be installed to reduce the scattering from the radiator. Note that in the rate simulations described later in the proposal, the effective thickness of the radiator was assumed to be slightly larger, $t_{rad}/X_0 = 0.08$, due to additional radiative processes in the target and the virtual photon flux. This description is reproduced from the WACS proposal.

3.3. Deflection Magnet

Previous RCS experiments have shown that a deflection magnet provides an effective way to discriminate between elastic electron and photon scattering events. When a deflection magnet is used there is no need for a veto detector, which in turn allows for at least ten times higher photon/electron beam intensity. The deflection magnet for the new WACS experiment has been designed with a large enough aperture to cover the entire calorimeter and provide adequate electron deflection while minimizing the magnetic field on the beam line. The description of the magnet and its optimization procedure has been reproduced from the WACS proposal.

One of the key aspects in discriminating the signal from background, in both the

WACS and photopion experiments, is a reliable comparison of the expected and measured electron-proton (calorimeter-HMS) correlation. The angular spread of this correlation is smaller in the out-of-plane direction because it is defined only by angular resolution; in contrast, it is larger in-plane because its dominant contribution comes from the proton momentum reconstruction resolution for a given proton momentum. Typically the out-of-plane resolution relevant for the e-p correlation is twice as good as the in-plane resolution. The bending direction for elastic electrons should therefore be vertical (magnetic field horizontal) in order to minimize the required deflection of electrons and the resulting value of the field in the deflection magnet.

Additional information about the magnet design is presented in Ref. [11].

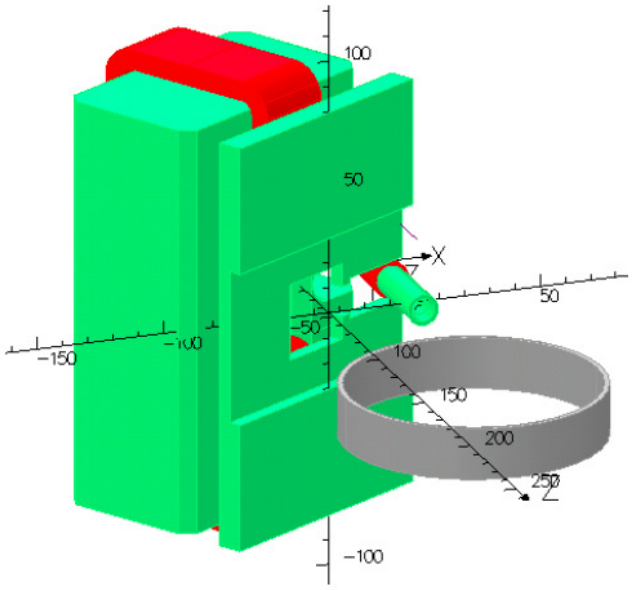

FIG. 8. An image of the deflection magnet for the WACS experiment from the TOSCA analysis package, with the magnet placed at a 30 degree scattering angle with 110 cm between the magnet center and the target. This image is reproduced from the WACS proposal.

In order to extract the π^0 cross section the shape of the pion related events need to be well understood. The deflector magnet must therefore relocate the electrons sufficiently far from the π^0 decay events. This can be accomplished by a sufficiently strong deflector magnet. A magnet that will be able to provide a field integral of up to $\int B \cdot dl \sim 0.6Tm$ has been designed and will be constructed for the proposed WACS experiment. It will be placed as shown in Fig. 7 and an image of the magnet is shown in Fig. 8. We will use the same magnet for the additional kinematics covered in this proposal.

3.4. The High Momentum Spectrometer

The recoil protons in the proposed experiment will be detected by the High-Momentum Spectrometer (HMS), which is part of the standard equipment of Hall C. The HMS is a high resolution ($\delta p/p < 10^3$) magnetic spectrometer in a QQQD magnet configuration with a maximum momentum of 7.5 GeV/c and a momentum bite of 18 %. It has an octagonal input aperture with an effective solid angle coverage of approximately 6 msr and can be positioned to angles greater than 12.5°. The detector package of the HMS consists of two vertical drift chamber packages for track reconstruction, scintillator hodoscopes for timing, as well as a gas C̈erenkov counter, an aerogel C̈erenkov counter, and a segmented lead-glass shower calorimeter for particle identification. If needed, the shower calorimeter could be used in the trigger. The HMS can be tuned in parallel-to-point mode (for optimal in-plane angle accuracy) or point-to-point mode (for best vertex reconstruction). In the proposed experiment it will be used in the latter mode in which extended targets can be accommodated with a vertex reconstruction accuracy of 1 mm, and where both in-plane and out-of-plane angle measurement resolutions are about 0.8 mrad. In this proposal the SIMC simulation package was used for determination of the

actual momentum and angular resolutions, which included scattering in the target material as well as reconstruction effects. The simulation is further elaborated in a later section. This description is reproduced from the WACS proposal.

3.4.1. Expected Rates

The DINREG Monte Carlo code developed by the RadCon group at JLab [41] has been used to calculate the expected proton and π^+ rates in the HMS for each of the proposed kinematic settings. Fig. 9 shows the simulated HMS singles rates, and the simulated proton-to-π^+ ratio. The maximum HMS singles rate is at kinematic point 3F, which will be run at a beam current of 15μA, and is around 75 kHz. The equivalent trigger rate (for protons only) for this same kinematic point is 7.5 kHz. These rates are well within the capabilities of the HMS.

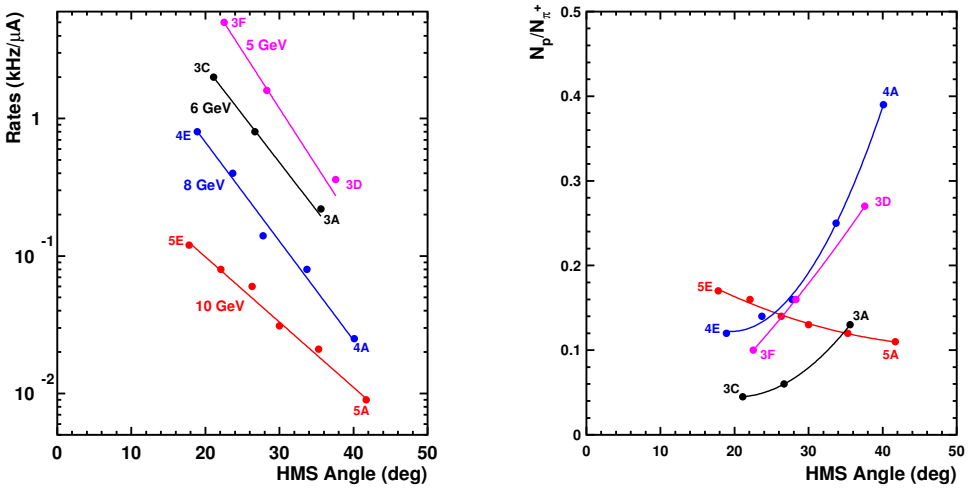

FIG. 9. Simulated raw singles rates in the HMS (left) and proton-to-π^+ ratio (right).

3.5. The Photon Calorimeter

The photon calorimeter for this experiment will be the new Neutral Particle Spectrometer [10] being constructed in Hall-C. This photon calorimeter will consist of a rectangular array of 31 (horz) $\times$ 36 (vert) $PbWO_4$ crystal blocks with dimensions $2.05 \times 2.05 \times 18$ cm^3. Each crystal is attached to a photomultiplier tube and base. The proposed calorimeter is based on the existing HYCAL calorimeter [42]. Fig. 10 shows an array of crystal blocks that will closely resemble the one that will be used in the proposed experiment.

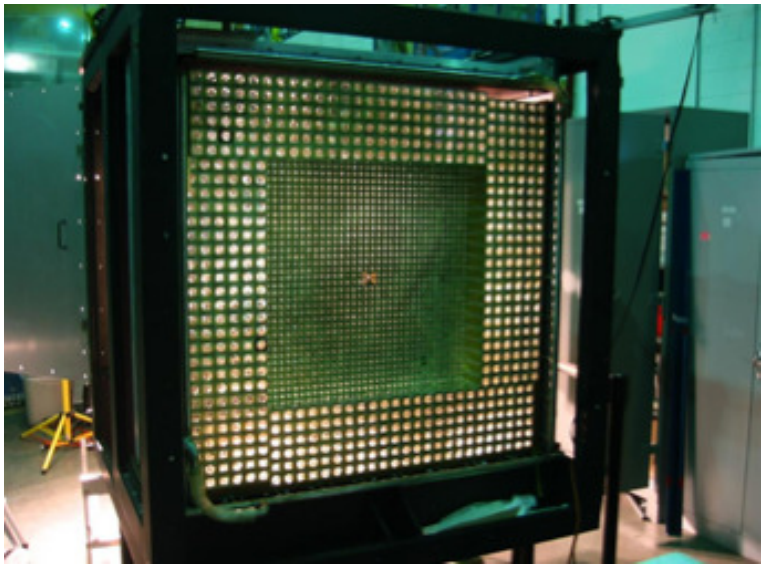

FIG. 10. The central high-resolution $PbWO_4$ part of the HYCAL detector will be used in the NPS.

The PMTs are shielded from ambient light in a light-tight box that contains an aircooling system, whose main purpose is to prevent the PMTs from overheating and aid in the overall stable operation of the calorimeter. The yield of the $PbWO_4$ crystals is temperature dependent, with $\approx 2\%/^{\circ}C$ deterioration of light yield around room temperature. HV and signal-cable systems are also contained in the light box

encasing the PMTs. The calorimeter will be equipped with a system that distributes light pulses to each calorimeter module. The main purpose of this system is to provide a quick way to check the detector operation and to calibrate the dependence of the signal amplitudes on the applied HV. The detector response to photons of a given energy may drift with time, due to drifts in the PMT gains and to changes in the glass transparency caused by radiation damage. For this reason, the gain monitoring system will also allow measurements of the relative gains of all detector channels during the experiment. The calorimeter can be moved into the hall without being disconnected from the frontend electronics, which is located in racks a few feet behind the main detector components. The position of the photon arm will be adjusted for each kinematics to match the angular position of the HMS. The calorimeter will most likely be placed on rails and repositioned by sliding along these rails. To shield from radiation it will be very beneficial to place a 10 cm thick plastic cover with an effective surface area thickness of approximately $10 g/cm^2$ in front of the calorimeter. This description is reproduced from the WACS proposal.

3.5.1. Expected Rates

DINREG Monte Carlo simulations for the expected NPS singles rates have also been performed for each of the proposed kinematic points [41]. The total number of γ, e^+ and e^- incident on the calorimeter with energy greater than 1 GeV gives a maximum singles rate of 1.2 MHz. The simulated rates are shown in Fig. 11.

3.6. Trigger and DAQ

The HMS trigger will be the only trigger for this experiment, this is possible because of the modest event rate expected in the proton arm at high photon beam energies and because the new HMS and NPS pipeline based electronics will be dead-

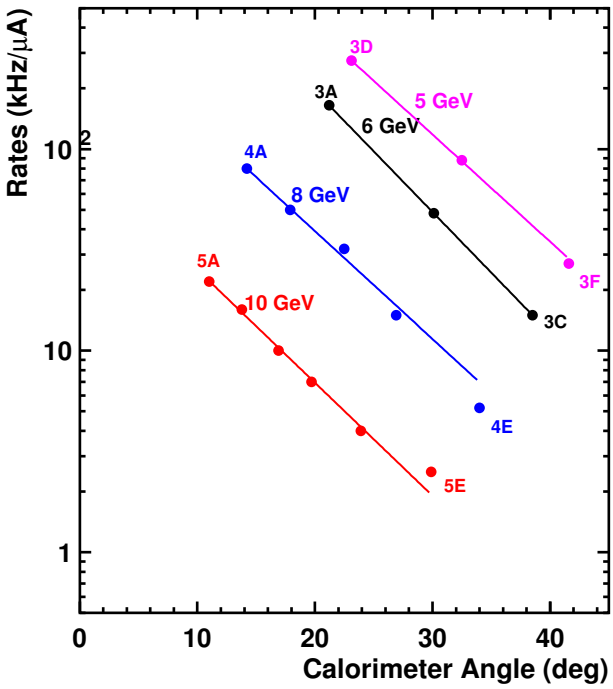

FIG. 11. Simulated raw singles rates in the NPS

.

time free. Hence each particle detected by the HMS will trigger the DAQ readout of both the HMS and the calorimeter. The cluster summing trigger for the calorimeter will not be implemented. The read-out of the NPS FADCs will be controlled by FPGA based hardware, which will be programmed to recognise where a hit has occurred and will read out only the relevant group of FADC modules. This will avoid generation of extraneous data.

The typical NPS event size is expected to be 1 kB, while the HMS event size is expected to be less than 2 kB [11]. Since the trigger will be formed by the HMS, the maximum data throughput will be at kinematic point 4E where, the expected trigger rate is7 kHz. These numbers, along with the expected NPS singles rates

gives the a maximum DAQ rate of $\sim$ 2 MB/s and a total dataset of around 1 TB. Both these numbers are well within the capabilities of the online DAQ and data storage facilities. This description is reproduced from the WACS proposal.

3.7. Radiation Budget

The high luminosity required in the proposed experiment could result in loss of the energy and coordinate resolutions of the calorimeter due to pileup. Long operation at high radiation load could cause radiation damage to the crystals and loss of their performance.

In order to estimate the potential for radiation damage to the calorimeter crystals, the DINREG simulation code was used. The total dose rate incident upon the NPS calorimeter for each kinematic point and the proposed running conditions has been calculated, with the results shown in Fig. 12. The maximum expected rate is 840 rad/h for kinematic point 4D. Assuming the dose is deposited over the full crystal length, this simulation gives a total accumulated dose estimate for the full beam-time of 153 kRad. This does not include the effects of shielding the calorimeter from low energy electromagnetic radiation, with shielding the radiation does radiation dose is expected to be 45 krad. Although these numbers are signicant, they are still acceptable according to a study [44], which found that at a value of 1 Mrad, the light output reduction for $PbWO_4$ is around 2%.

Using the data from the previous RCS experiment in 2002, the radiation level in Hall C during the proposed experiment is expected to be of the order of 200 mR/hour. The radiation load could be reduced by a factor of 2, if necessary, by using modest local shielding of the radiator and the target installed at angles above 50°. This description is reproduced from the WACS proposal.

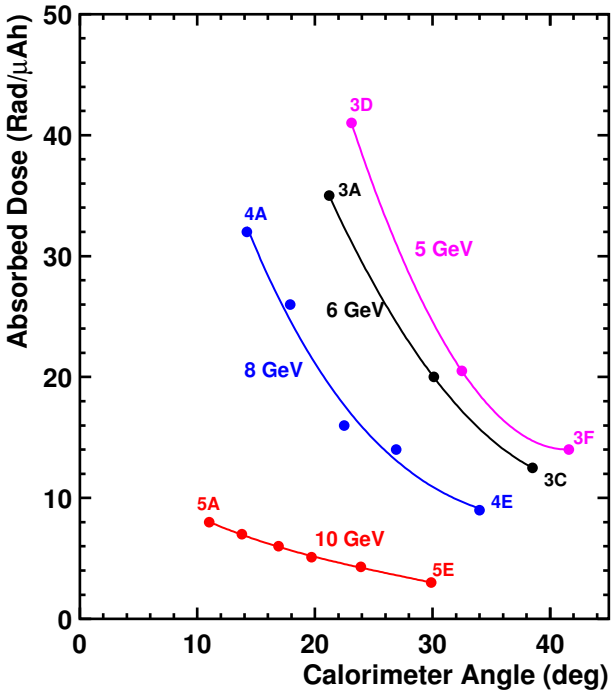

FIG. 12. Simulated radiation dose in the NPS.

.

3.8. Energy and Coordinate Resolution

The energy of the particle detected in the calorimeter is calculated from a sum of the signals in several crystals (up to 9) which form a cluster. The noise in the ADC used for a measurement of the signal from an individual crystal contributes to the detector energy resolution. In a high-rate experiment the ADC noise is increased, and this can be characterized by the ADC pedestal width. Using the observed 5-6 MeV pedestal width observed in the previous RCS experiment, the expected pedestal width for the this proposal is projected to be around 50 MeV. The effect of the background on the energy resolution could be estimated from this estimated

pedestal width and the number of modules in the cluster. It is expected to be on the level of 110-150 MeV or 3.3-4.5%, a similar estimate shows that the effect on the coordinate resolution is around 0.5 mm. This description is reproduced from the WACS proposal.

3.9. Kinematic settings

The differential cross section for Wide-angle π^0 photoproduction will be determined at photon energies of 5.0 - 10.0 GeV at $50^\circ < \theta_{cm} < 105^\circ$. The kinematic for two standard beam energies of 8.8 GeV and 11 GeV is exactly indentical to those for the new proposed WACS experiment. However, unlike the WACS experiment the π^0 experiment will measure the cross section at one additional setting at beam energy of 11.0 GeV and a third standard beam energy of 6.6 GeV. The kinematics for only the additional settings at 11.- GeV and 6.6 GeV beam are shown in Table I, the kinematics settings at 8.8 and 11 GeV that are identical to the WACS experiment are not shown here. The coverage in $|t|$ and s for full experiment is shown in Fig. 13. In all cases, the scattering angles and momenta fall well within the allowed range for the HMS and the NPS and pose no practical difficulties in terms of positioning of the detector systems.

3.10. Monte Carlo Simulation

The WACS collaboration has developed a Monte Carlo simulation in order to study the feasibility of extracting the RCS signal from large backgrounds due to the π^0 decay and elastic e-p scattering. Events are first generated over a much broader kinematic range compared to the detector acceptances, according to cross section parameterizations of the three reaction types: RCS, neutral pion photoproduction, and elastic *ep* scattering. We have used this same Monte Carlo simulation for our

TABLE I. Table of kinematics for the $p(\gamma, \pi^0 p)$ reaction at $\mathrm{E_{beam}}$ of 11.0 at pion c.m. angle of 90^o and 6.6 GeV at pion c.m. angle of 70, 90 and 105^o. These settings are in addition to the setting used in the WACS proposal.

	E_γ	θ^π_{cm}	$\sqrt{s}$	$\lvert t\rvert$	θ_p (lab)	θ_{π^0} (lab)	P_p	P_{π^0}
3A	6.0	70	3.48	3.44	35.6	21.2	2.602	4.170
3B	6.0	90	3.48	5.21	26.7	30.1	3.595	3.218
3C	6.0	105	3.48	6.98	21.1	38.5	4.334	2.50
3D	5.0	70	3.20	3.14	37.6	23.1	2.251	3.497
3E	5.0	90	3.20	4.81	28.3	32.5	3.079	2.716
3F	5.0	105	3.20	5.32	22.5	41.6	3.691	2.125
5F	10.0	90	4.43	8.01	22.1	23.9	5.632	5.227

studies. In order to study the feasibility of extracting the photoproduced π^0, we have added two more reactions 2-pion production and η production. The parameterizations of the cross sections are based on E99-114 data in the case of RCS and neutral pion photoproduction [45] and the Bosted fit to the Sachs form factors for elastic *ep* scattering events [46]. The 2-pion and η production cross sections were obtained from the Durham database [47]. The proton interactions in the target and HMS are then simulated using the standard Hall C SIMC simulation package, while the particles scattered towards the NPS (photons, pions and electrons) are simulated using dedicated software developed within the CERN Geant4 framework. This latter tool includes a realistic simulation of the target, scattering chamber, deflection magnet and the NPS. The technique developed and refined for identifying RCS events and extracting the associated yield, namely, one assumes two-body kinematics and uses the measured recoil proton variables to reconstruct a predicted hit position for the corresponding scattered photon at the NPS. The differences between the predicted

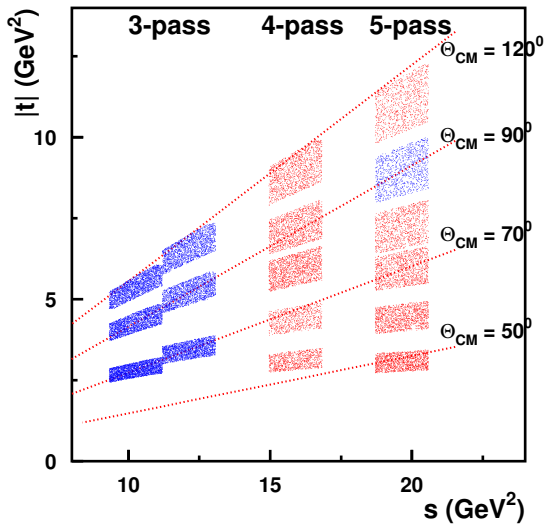

FIG. 13. Kinematic coverage with the 3 pass, 4 pass and 5 pass beams, determined by the HMS acceptance and a photon energy range of 1 GeV about the central setting. The WACS settings are shown in red while the π^0 only settings are shown in blue.

.

and measured NPS hit positions, δx and δy, are then used to identify the reaction from which a particular event originated. The distributions shown in Figs. 14 (obtrained from the WACS collaboration) correspond to the difference between the expected NPS hit positions for a good proton track in the HMS and the center-of-gravity positions of the highest energy NPS cluster. One can see that the elastic ep events are centered at positive δy due to deflection in the magnet, RCS events are centered around zero, and events from detection of one of the photons from the decay of a neutral pion form a relatively broad background.

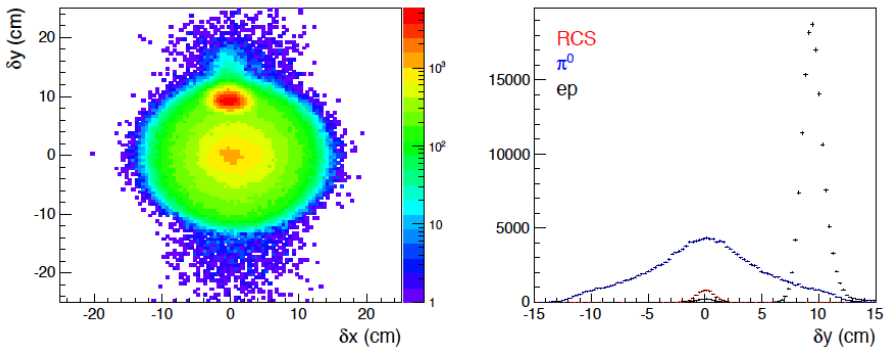

FIG. 14. Typical NPS hit difference distributions for kinematic point 4D. (Left)δx vs δy for all events. (Right) A projection on to δy for events in the central δx region. Figure obtained from WACS collaboration.

.

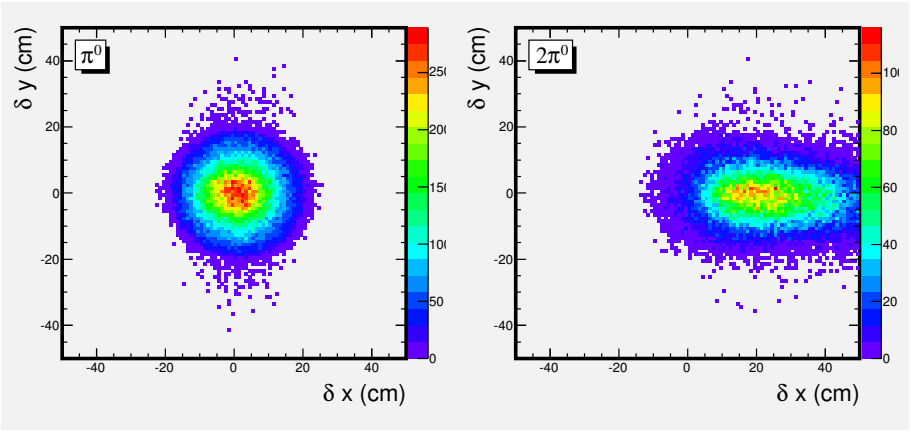

FIG. 15. (Left)δx vs δy for π^0 events for kinematic point 3B. (Right) δx vs δy for 2-π^0 events.

The same technique was found to work very well in distinguishing 1-pion from 2-pion events. In Fig. 15 we compare the δx and δy for single pion (left) and two pion (right) events. The photons from the decay of 2-pion events have relatively large δx, and once a cut corresponding to $\pm 1.5\sigma_x$ (where σ_x is the x-resolution of

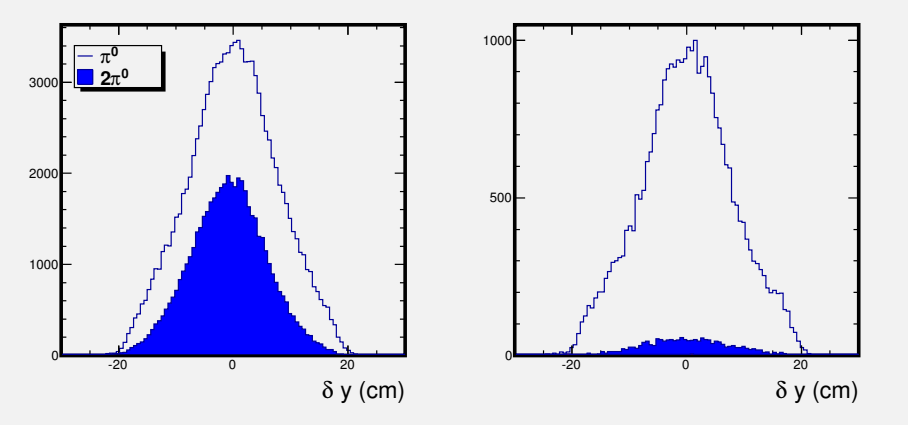

FIG. 16. Left:A projection on to δy for all π^0 and 2-π^0 events (shaded). Right: A projection on to δy for π^0 and 2-π^0 events (shaded) in the central δx region.

the calorimeter) is applied, very few of the 2-pion events end up being wrongly identified as 1-pion events, as seen in Fig. 16. These figures are for the situation with the worst $2-\pi/\pi$ ratio (kinematics 3F), and demonstrate that the technique is very effective in rejecting $2-\pi$ events. A more typical situation corresponding to kinematics 5B is shown in Fig. 17

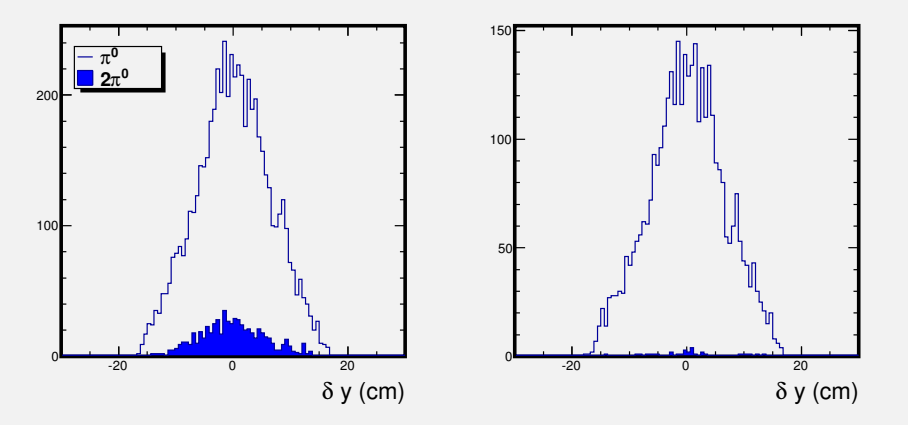

FIG. 17. Left:A projection on to δy for all π^0 and 2-π^0 events (shaded). Right: A projection on to δy for π^0 and 2-π^0 events (shaded) in the central δx region.

Above the η production threshold, the η events are indistinguishable from the 1-pion events, however the η production rates were negligible compared to the 1-pion rates. Fig. 18 shows all the η events detected (left) for the kinematics with the worst η/π^0 ratio (5D) and the events which survive the cut corresponding to $\pm 1.5\sigma_x$ (right), which are $< 1\%$ of the π^0 events.

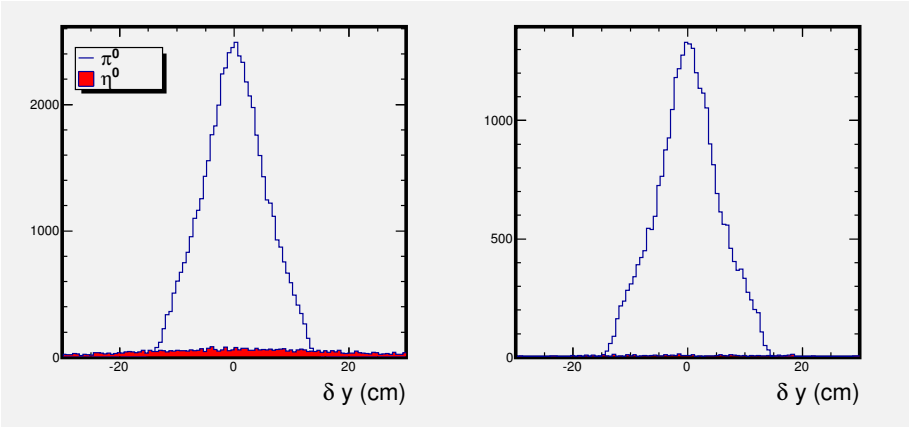

FIG. 18. Left:A projection on to δy for all π^0 and η events (shaded). Right: A projection on to δy for π^0 and η events (shaded) in the central δx region.

The free parameters associated with the experimental set-up i.e. the deflection magnet distance and field integral, as well as the NPS distance have been optimized with the Monte Carlo simulation for all kinematic settings in order to maximize the deflection of the electrons from *ep* events, minimize the resolution of the NPS hit difference distributions as well as the relative number of background events compared to the signal. The optimized values of the parameters of the experimental settings for the 6.6 GeV settings are shown in Table III. The parameters for the 8.8 and 11 GeV settings are identical to the WACS proposal [11] and are not repeated here.

Another interesting feature of this experiment will involve the dual role for the events close to the end point of the Bremsstrahlung spectrum which is well below the two pion threshold. For these π^0 events there are no 2-pion or η backgrounds.

Therefore, these events can also be used to optimize and then monitor the π^0 acceptance and efficiency of the calorimeter. The measured π^0 acceptance function can then be used to build better simulations of the calorimeter.

3.10.1. Physics Background

Although the deflection magnet deflects the *ep* elastic events away from the RCS peak it does not deflect it completely outside the NPS acceptance. Thus the *ep* events are the dominant background for the extraction of the π^0 yield. The ratio N_{ep}/N_{π^0} varies between 0.02 - 4.87, while the N_{RCS}/N_{π^0} varies between 0.07 - 2.17. Experience from previous JLab WCS experiments has shown that good calorimeter energy resolution, two-cluster analysis along with a Monte Carlo simulation can be used to fit the pion, the RCS and the *ep* events and extract the pion yield. For this reason, one other critical factor in the final values chosen for the NPS distance has been to ensure that the distribution of pion events in δx and δy is not artificially truncated by the NPS acceptance. The feasibility of separating the π^0 events from the RCS events is shown for each kinematics in the WACS proposal [11] and is not reproduced here. However, unlike the WACS experiment, 2π and η events are additional physics backgrounds in extracting the π^0 cross section. The ratio $N_{2\pi^0}/N_{\pi^0}$ varies between 0.012 - 0.053 and the N_{η}/N_{π^0} varies between 0.001 - 0.012, in the $1.5\sigma_x$ central δx - δy region. These cannot be the distinguished from the single pion events and will lead to an additional systematic uncertainty compared to the WACS experiment. Contribution from these events will be corrected for using an estimate from a Monte Carlo simulation.

3.10.2. Detector Resolution

Based on the experience from previous JLab WACS experiments, it has been established that the two-arm resolution for the calorimeter hit difference distributions, is dominated by i) proton multiple scattering and reconstruction in the proton spectrometer, and ii) the out-of-plane (δy) resolution is much better than the in-plane (δx) resolution, as a result of the fact that the latter includes significant contributions from the proton momentum and vertex resolutions. This is the primary reason that a horizontal magnetic field, and therefore vertical deflection, is critical to the success of the proposed measurements. Typical values for the expected NPS position and energy resolutions have been included in the Monte Carlo simulation, as have photon/electron interactions in the target, scattering chamber and a 10-cm plastic shield directly in front of the NPS which acts as a shield from low energy electromagnetic background. These result in a contribution to the resolution over all kinematic settings of around 0.35 cm. For the range of proton momenta considered in the present proposal (1.791 - 7.586 GeV/c), the in-plane angular resolution varies between 1.5 and 2.5 mrad, the out-of-plane resolution between 1.7 and 3.8 mrad, and the $\delta p/p$ resolution between 5 and 7.5×10^4. It is primarily the last (although there is a small contribution from the vertex resolution) that leads to the δx resolution being poorer than the δy resolution. The NPS distance clearly plays a crucial role in determining the final values for the two-arm resolutions. It has therefore been optimized for all kinematic settings such that the out-of-plane resolution remains around or less than 1 cm at the two highest beam energies and less than 2 cm for the setting using the 6.6 GeV beam. The table of parameters for the experimental setup is shown in Tables II and III. The $\mathrm{E_{beam}}$ = 8.8 and 11 GeV are identical to the WACS experiment [11]. This description is reproduced from the WACS proposal.

TABLE II. Table of parameters for the experimental setup for the E_{beam} = 8.8 and 11 GeV settings where the π^0 cross section will be exracted. These are reproduced from the WACS proposal, except for the additional setting 5F to cover the 90° c.m. angle at the highest photon energy.

Label	D_{NPS}	D_{mag}	B	σ_x	σ_y	e-defl	$N_{ep\gamma}/N_{\pi^0}$	$N_{\pi^0\pi^0}/N_{\pi^0}$	N_{η}/N_{π^0}	N_{RCS}/N_{π^0}
	(m)	(m)	(T)	(cm)	(cm)	(cm)				
4B	7.0	1.65	1.00	2.21	0.75	10.74	1.12	0.022	0.006	0.90
4C	5.0	1.65	1.25	1.61	0.71	9.55	0.29	0.018	0.004	0.37
4D	3.5	1.10	1.50	1.36	0.79	9.24	0.11	0.021	0.004	0.21
4E	3.0	1.10	1.50	1.21	0.86	8.72	0.03	0.022	0.006	0.1
5B	9.0	2.45	0.875	2.63	0.71	8.71	4.18	0.012	0.012	1.39
5C	7.0	1.65	1.00	2.30	0.77	9.75	0.97	0.012	0.004	0.56
5D	6.0	1.65	1.25	2.18	0.79	9.91	0.69	0.012	0.008	0.36
5E	3.25	1.10	1.50	1.26	0.92	8.07	0.03	0.017	0.006	0.08
5F	5.0	1.10	1.50	2.16	0.82	9.57	0.43	0.015	0.006	0.22

3.11. Rates and Systematic Uncertainties

The expected RCS event rate for the kinematic settings given in Tables 2 has been calculated with the Monte Carlo simulation and yield extraction analysis technique described above. The event rate is the product of the luminosity, the cross section, and the acceptances of the detectors, as well as all other factors such as DAQ dead time, efficiency of the trigger, and the detectors and efficiency of the reconstruction analysis. The rate was calculated as:

$$N_{\pi^0} = \frac{d\sigma}{dt}\frac{(E_\gamma^f)^2}{\pi}\Delta\Omega_\gamma f_{\gamma p}\left(\frac{\Delta E_\gamma^f}{E_\gamma^f}\frac{t_{rad}}{X_0}\right)\mathcal{L}_{ep},$$

TABLE III. Table of parameters for the experimental setup for the E_{beam} of 6.6 GeV settings. These are in addition to the settings of the WACS experiment.

Label	D_{NPS}	D_{mag}	B	σ_x	σ_y	e-defl	$N_{ep\gamma}/N_{\pi^0}$	$N_{\pi^0\pi^0}/N_{\pi^0}$	N_{η}/N_{π^0}	N_{RCS}/N_{π^0}
	(m)	(m)	(T)	(cm)	(cm)	(cm)				
3A	5.0	1.1	1.25	2.27	0.89	12.8	0.25	0.020	0.002	0.41
3B	3.5	1.1	1.5	1.51	0.87	11.3	0.05	0.033	0.001	0.15
3C	3.0	1.1	1.5	1.40	0.82	10.2	0.026	0.039	0.001	0.076
3D	5.0	1.1	1.25	2.46	0.97	14.9	0.31	0.04	0.001	0.57
3E	3.5	1.1	1.5	1.55	0.96	12.9	0.052	0.052	0.001	0.19
3F	3.0	1.1	1.5	1.51	1.12	11.64	0.02	0.053	0.001	0.07

where $\frac{d\sigma}{dt}$ is the photopion cross section, the factor $\frac{(E_\gamma^f)^2}{\pi}\Delta\Omega_\gamma$ is the range of Δt for a given kinematics, $f_{\gamma p}$ is the fraction of events detected for a given range of photon energies E_γ^f, $\frac{\Delta E_\gamma^f}{E_\gamma^f}\frac{t_{rad}}{X_0}$ is the photon flux, i.e. the number of photons produced per incident electron (including photons produced in the target and virtual photons), and $\mathcal{L}_{ep}$ is the electron-proton luminosity.

The statistical precision that can be achieved, including the uncertainty due to the fluctuations in the $ep\gamma$ and RCS background is given by:

$$\delta_{stat} = \frac{\delta_{N_{\pi^0}}}{N_{\pi^0}} = \frac{\sqrt{(N_{\pi^0} + R_{ep\gamma}N_{\pi^0} + R_{RCS}N_{\pi^0})}}{N_{\pi^0}}$$

The raw singles rates in the HMS and NPS have been determined for events arising from RCS, elastic ep scattering and π^0 photoproduction. The HMS singles rates for π^+ photoproduction have also been calculated. These are shown for a corresponding electron beam current chosen for each kinematic setting in Tables IV and V. For all settings the HMS trigger rate will be well within acceptable HMS operating parameters as determined in previous HMS experiments. The π^+ rates are such

that rejection of these events off-line via the kinematic reconstruction technique described in previous sections will be sufficient, without the need for any additional particle identification. This description is reproduced from the WACS proposal.

TABLE IV. Table of rates for the E_{beam} = 8.8 and 11 GeV settings. These are exactly the same as the settings for the WACS experiment except for setting 5F which is new. The beam time includes 7 hours for runs with radiator removed and for spectrometer moves. For setting 5F the overhead is only 3 hrs which includes 1 hr for runs without the radiator and 2 hrs for spetrometer move.

/

Label	I_{beam}	$\dot{N}_{\pi^0}$	N_{π^0}	δ_{stat}	t
	(μA)	($\mu A^{-1} hr^{-1}$)		%	(hr)
4A	5	6.9	700	11	20+7
4B	15	6.7	2000	4	20+7
4C	30	8.1	4900	1.8	20+7
4D	60	6.9	12400	1.0	30+7
4E	60	7.1	17000	0.8	40+7
5A	15	2.7	800	15.7	20+7
5B	30	2.2	1600	6.4	25+7
5C	60	2.9	3400	2.7	20+7
5D	60	2.8	6600	1.8	40+7
5E	60	3.8	27000	0.6	120+7
5F	60	3.2	1000	4.1	5+3
Total					433

The three main sources of systematic uncertainties in the proposed measurement

TABLE V. Table of rates for the E_{beam} of 6.6 GeV settings. The beam time includes 1 hr for runs with radiator removed and 2 hrs for spectrometer moves.

Label	I_{beam}	$\dot{N}_{\pi^0}$	N_{π^0}	δ_{stat}	t
	(μA)	($\mu A^{-1} hr^{-1}$)		%	(hr)
3A	15	31.1	2300	2.7	5+3
3B	15	45.4	3400	1.6	5+3
3C	30	48.2	7200	1.2	5+3
3D	15	45.1	3400	2.4	5+3
3E	15	59.4	4400	1.7	5+3
3F	15	59.5	4400	1.6	5+3
Total					48

of the π^0 cross section are those associated with the yield extraction, the determination of the detector acceptance and efficiencies, and the determination of the total photon beam flux. The extensive experience gained during the E99-114 and E07-002 experiments in combination with the Monte Carlo simulation studies detailed in the previous section is relied upon to make estimates of these various sources of systematic uncertainties. Adding the various contributions described below in quadrature, it is estimated that the total systematic uncertainty for the proposed measurement will be around 8% for the least favorable kinematic setting. Beginning with the total photon beam flux, there are contributions to this particular uncertainty from measurement of the accumulated electron beam charge, target thickness, and determination of the bremsstrahlung photon flux for a given energy range. This last dominates, while the others are estimated to be less than 1%. The utilization of redundant calculations of the bremsstrahlung flux (using both Geant4 and dedicated

thick-target bremsstrahlung tools) and measurements using the actual data lead to confidence that this uncertainty can be kept around the 3% level. Furthermore, previous experience working with the HMS, the simple geometry of the NPS, and the fact that the HMS will be operating well within its capabilities lead to the expectation that the systematic uncertainty associated with detector acceptances and efficiencies will be around the same 3% level. The extraction of the π^0 yield will have uncertainties from the RCS, ep, 2π and η backgrounds, which vary relative to each other for different kinematic settings. In order to estimate the magnitude of the systematic errors arising as a result of contamination from these background sources (as given by the ratios in Table. II,and III), we have relied on the analysis of the RCS collaboration. Since the 2π and η contaminations are small, the major contributions to the uncertainty are from the ep and RCS contaminations and are therefore same as those for the RCS experiment. Based on the Monte Carlo simulations an additional 1-5% (depending $N_{2\pi}/N_{\pi}$) uncertainty is assigned due to background from 2π and η (assuming 100% uncertainty in the subraction of this background). A list of systematic uncertainties is shown in Table VI. Most of this description is reproduced from the WACS proposal. The total estimated uncertainty for each of the kinematic settings where the π^0 cross section will be extracted is shown in Table. VII.

3.12. Beam Time Request

A bulk of the beam-time request is just the beam time requested by the WACS proposal. The beam time request for the additional 11 GeV and the 6.6 GeV kinematics is based on time needed to achieve a combined uncertainty of < 10 %. These numbers have been calculated based on the expected rates given in the previous section and include estimated overheads from background measurements without

TABLE VI. Table of estimated systematic uncertainties for the π^0 cross section measurement. The total is the quarature sum.

Source	Uncertainties
	%
Beam charge	1.0
Target thickness	1.0
Bremsstrahlung flux	3.0
NPS efficiency	1.5
HMS efficiency	1.5
HMS tracking efficiency	1.5
RCS background	3.0
$ep\gamma$ background	3.0
$2\pi, \eta$ background	1.0 - 5.0
Total	6.1 - 7.8

the radiator and configuration changes between kinematic settings. The beam-time estimate for the 4-pass kinematic settings and 5-pass settings are exactly same those for the WACS experiment (i.e. 425 hrs), since the π^0 data will be collected at the same time as the WACS experiment. The additional beam-time needed for the single 5-pass setting and the 3-pass settings is **56 hours** over the 7 different settings. The net total beamtime request including the common time with the WACS experiment is 481 hrs ($\sim$ 20 day).

TABLE VII. Table of estimated total uncertainty (quadrature sum of systematic and statistical) for the each of the kinematic settings where the π^0 cross section will be extracted.

Setting	Uncertainty	Setting	Uncertainty	Setting	Uncertainty	Setting	Uncertainty
	%		%		%		%
5B	8.9	4B	7.6	3A	6.9	3D	7.6
5C	6.7	4C	6.5	3B	7.0	3E	8.1
5D	6.4	4D	6.4	3C	7.3	3F	8.2
5E	6.3	4E	6.5				
5F	7.4						

3.13. Projected Results

The π^0 photoproduction cross sections measured in this experiment will cover a large range of c.m. energy overlapping with previous measurements at $s < 10GeV^2$, and extending up $s \sim 20GeV^2$. These results may help resolve the discrepancy between the previous measurements. Fig. 20 shows the projected results at 70^o, 90^o and 110^o c.m. angles.

4. SUMMARY

The $\gamma p \to \pi^0 p$ process is one of the simplest exclusive processes to investigate the dominance of the handbag mechanism, and to study the onset of scaling behavior for π^0 photoproduction. Utilizing fully the advantages of high luminosity and the energy upgraded CEBAF. The slower decrease of the differential cross-section for the process compared with many other photon induced two-body processes allows differential cross-section measurements all the way to the highest possible center-

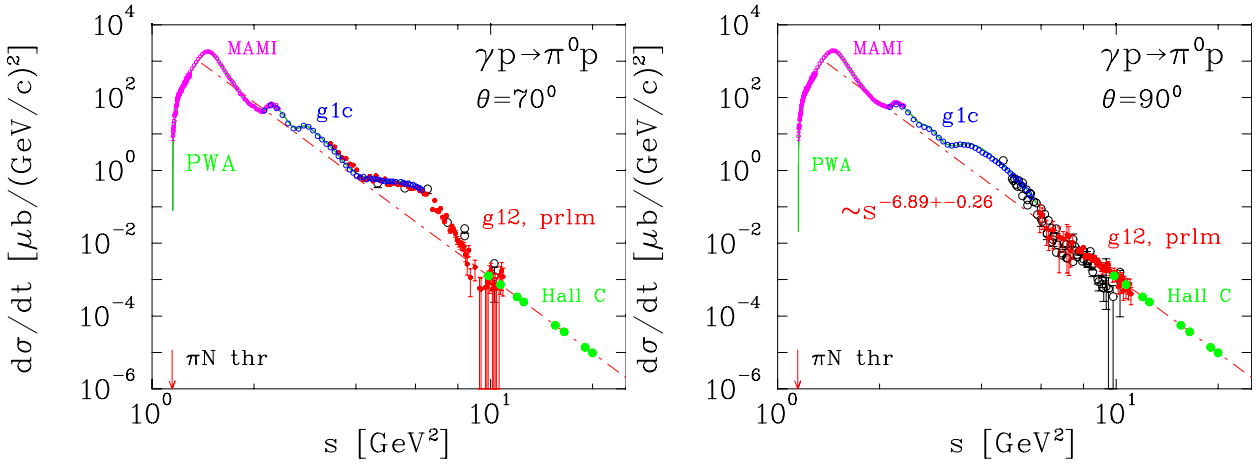

FIG. 19. Projected results at 70° and 90° c.m. angle.

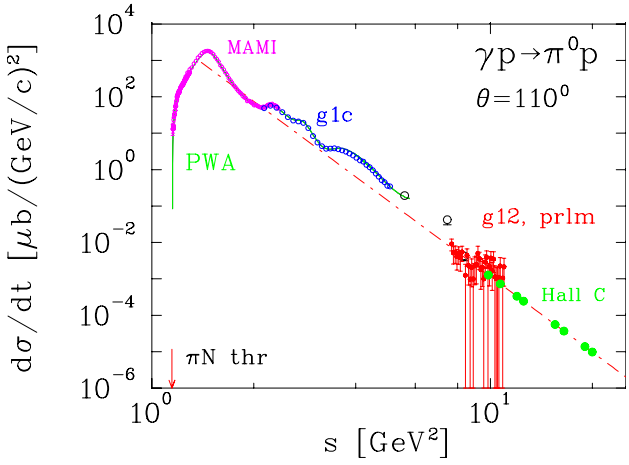

FIG. 20. Projected results at 110°.

of-mass energy with a 11 GeV CEBAF beam. Specifically, a 11 GeV beam will allow:

- A precise measurement of the π^0 photoproduction cross section at the highest energies available, to help resolve some of the discrepancies between the previous measurements.

- Detailed investigation of the angular dependent scaling onset will help understand the origin of scaling behavior.

- Investigate the deviations from scaling behavior and oscillations as suggested by results [24] on charged pions.

---

[1] X. Ji, Phys. Rev. Lett. **78**, 610 (1997); Phys. Rev. D **55**, 7114 (1997); A.V. Radyushkin, Phys. Lett. **B380**, 417 (1996); Phys. Rev. D **56**, 5524 (1997); M. Diehl, T. Feldmann, R. Jakob, P. Kroll, Eur. Phys. J. **C 8**, 409 (1999).

[2] A. V. Radyushkin, Phys. Rev. **D 58**, 114008 (1998) [hep-ph/9803316].

[3] M. Diehl, T. Feldman, R. Jacob, P. Kroll, Eur. Phys. J. **C 8**, 409 (1999) [hep-ph/9811253].

[4] H. W. Huang, P. Kroll, Eur. Phys. J **C 17**, 423 (2000) [hep-ph/0005318].

[5] N. Kivel and M. Vanderhaeghen, JHEP **04**, 029 (2013); arXiv:1212.0683; arXiv:1312.5456.

[6] H. W. Huang, P. Kroll, T. Morii, Eur. Phys. J. C **23**, 301 (2002).

[7] M. Diehl and P. Kroll, Eur. Phys. J. C 73, 2397 (2013); arXiv:1302.4604.

[8] G. Eichmann and C. S. Fischer, Phys. Rev. D 87 , 036006 (2013); arXiv:1212.1761.

[9] H. W. Huang, R. Jacob, P. Kroll, K. Passek-Kumericki, Eur. Phys. J **C 33**, 91 (2004); P. Kroll private communication.

[10] R. Ent, T. Horn, H. Mkrtchyan *et al.*, Neutral-Pion Spectrometer Facility in Hall C, proposal to Jefferson Lab PAC 40.

[11] B. Wojtsekhowski, D. J. Hamilton, S.Širca *et al.*, Wide-angle Compton scattering at 8 and 10 GeV photon energies, proposal to Jefferson Lab PAC 41.

[12] C. White *et al.*, Phys. Rev. **D49**, 58 (1994).

[13] S.J. Brodsky and G.R. Farrar, Phys. Rev. Lett.**31**, 1153 (1973); Phys. Rev. D **11**, 1309 (1975); V. Matveev *et al.*, Nuovo Cimento Lett. **7**, 719 (1973);

[14] G.P. Lepage, and S.J. Brodsky, Phys. Rev. D **22**, 2157 (1980).

[15] T. Gousset, B. Pire and J. P. Ralston, *Phys. Rev.* D **53**, 1202 (1996).

[16] N. Isgur and C. Llewelyn-Smith, Phys. Rev. Lett. **52**, 1080 (1984).

[17] X. Ji, J.-P. Ma and F. Yuan, Phys. Rev. Lett. **90**, 241601 (2003).

[18] J. Polchinski and M.J. Strassler, Phys. Rev. Lett. **88**, 031601 (2002); R.C. Brower and C.I. Tan, Nucl. Phys. B **662**, 393 (2003); O. Andreev, Phys. Rev. D **67**, 046001 (2003).

[19] S. J. Brodsky and G. F. de Teramond, Phys. Lett. **B582**, 211 (2004); S. J. Brodsky *et al.*, Phys. Rev. D **69**, 076001 (2004).

[20] M. Fuchs et al, Phys Lett B 368, 20 (1996); R. Beck et al, Eur Phys J A 28S1, 173 (2006).

[21] M. Dugger et al., PRC 76, 025211 (2007); M. Dugger *et al.*, Phys. Rev. **C79**, 065206 (2009).

[22] M. Kunkel et al., Preliminary (2014).

[23] P. Joos, Preprint DESY-HERA 70-1, (1970).

[24] L. Y. Zhu *et al.*, Phys. Rev. Lett. **91**, 022003 (2003); L. Y. Zhu *et al.*, nucl-exp/0409018.

[25] W. Chen *et al.*, Phys. Rev. Lett. **103**, 012301 (2009).

[26] R. A. Arndt, W. J. Briscoe, R. L. Workman, and I. I. Strakovsky, the GWU CNS Database, http://gwdac. phys.gwu.edu/analysis/pr_analysis.html

[27] A. Sibirtsev, J. Haidenbauer, S. Krewald, T.-S. H. Lee, U.-G. Meissner, and A. W. Thomas, Eur. Phys. J. A 34, 49 (2007); A. Sibirtsev (private communications).

[28] R.L. Anderson *et al.*, Phys. Rev. **D14**, 679 (1976).

[29] "Photoproduction of Elementary Particles", edited by H. Genzel, P. Joos and W. Pfeil pp16-268, (1973).

[30] J. Napolitano *et al.*, *Phys. Rev. Lett.* **61**, 2530 (1988); S.J. Freedman *et al.*, *Phys. Rev.* C **48**, 1864 (1993); J.E. Belz *et al.*, *Phys. Rev. Lett.* **74**, 646 (1995).

[31] C. Bochna *et al.*, *Phys. Rev. Lett.* **81**, 4576 (1998).

[32] E.C. Schulte, *et al.*, *Phys. Rev. Lett.* **87**, 102302 (2001);

[33] P. Rossi *et al.*, Phys. Rev. Lett. **94**, 012301 (2005); M. Mirazita *et al.*, Phys. Rev. C **70**, 014005 (2004).

[34] K. Wijesooriya, *et al.*, *Phys. Rev. Lett.* **86**, , (2)975 (2001).

[35] K. Wijesooriya, *et al.*, *Phys. Rev.* C **66**, , (0)34614 (2002).

[36] W. Luo *et al. Phys. Rev. Lett.* **108**, , (2)22004 (2012)

[37] P. V. Landshoff, Phys. Rev. D **10**, 1024 (1974).
A.W. Hendry, Phys. Rev. D **10**, 2300 (1974).
D.G. Crabb *et al.*, Phys. Rev. Lett. **41**, 1257 (1978).

[38] Q. Zhao and F. E. Close, Phys. Rev. Lett. **91**, 022004 (2003).

[39] A. V. Belitski, X. Ji and F. Yuan, Phys. Rev. Lett. **91**, 092003 (2003).

[40] M. K. Jones *et al.*, Phys. Rev. Lett. **84**, 1398 (2000); O. Gayou *et al.*, Phys. Rev. Lett. **88**, 092301 (2002).

[41] P. Degtiarenco private communication.

[42] M. Kubantsev *et al.*. Performance of the Primex Electromagnetic Calorimeter, arxiv:physics/0609201, Sept 22, 2006; A. Gasparyan, Performance of PWO crystal detector for a High Resolution Hybrid Electromagnetic Calorimeter at Jefferson Lab, Proceed. X Int. Conf. on Calorimetry in Particle Physics, Perugia, Italy, 29 March - 2 April 2004, pp 109.

[43] David J. Hamilton, A simulation of the 12 GeV Hall C RCS experiment, University of Glasgow, April 14, 2013 (unpublished).

[44] Ren-yuan Zhu, Nucl. Instr. Meth. A 613 (1998) 297

[45] C. Hyde-Wright, A. Nathan, and B. Wojtsekhowski, spokespersons, JLab experiment E99-114.

[46] P.E. Bosted, Phys. Rev. C 51 (1995) 409.

[47] The Durham HepData Project; http://hepdata.cedar.ac.uk/reaction